Journal of Histochemistry & Cytochemistry 2019, Vol. 67(10) 723–734

DOI: 10.1369/0022155419859357
journals.sagepub.com/home/jhc
SAGE

Expression of IFT140 During Bone Development

Chenyang Zhang, Shuai Zhang, and Yao Sun
Department of Oral Implantology, School of Stomatology, Tongji University, Shanghai Engineering Research Center of Tooth Restoration and Regeneration, Shanghai, China (CZ, SZ, YS)

Summary
Primary cilia, hair-like organelles projecting from the surface of cells, are critical for sensing extracellular stimuli and transmitting molecular signals that regulate cell functions. During bone development, cell cilia are found in several types of cells, but their roles require further investigation. Intraflagellar transport (IFT) is essential for the formation and maintenance of most eukaryotic cilia. IFT140 is a core protein of the IFT-A complex. Mutations in IFT140 have been associated with cases of skeletal ciliopathies. In this study, we examined the expression of IFT140 during bone development. The results showed that, compared with many soft tissues, Ift140 (mRNA level) was highly expressed in bone. Moreover, its expression level was downregulated in the long bones of murine osteoporosis models. At the histological level, IFT140 was characteristically expressed in osteoblasts and chondrocytes at representative stages of bone development, and its expression level in these two types of cells was observed in two waves. These findings suggest that IFT140 may play an important role in the process of chondrogenic and osteogenic differentiation during bone development. (J Histochem Cytochem 67: 723–734, 2019)

Keywords
chondrocyte, cilia, differentiation, endochondral ossification, IFT, osteoblast, skeletal development

Introduction

Primary cilia, microtubule-based hair-like organelles projecting from the surface of most vertebrate cells,[1] are viewed as the antenna of the cells and the integration center of intracellular and extracellular signals.[2–6] Cilia are assembled by the process of intraflagellar transport (IFT), which is composed of more than 20 unique proteins and is organized in two complexes: IFT-B and IFT-A. They work as bidirectional trains for transportation along the cilia axoneme and are responsible for anterograde and retrograde trafficking, respectively.[7]

Alterations of many ciliary proteins can cause bone dysplasia and are classified as skeletal ciliopathies,[8,9] among which patients with mutations of IFT proteins are concentrated.[10] To date, mutations or alterations in genes encoding all six protein members of the IFT-A complex (IFT43, IFT121, IFT122, IFT139, IFT140, and IFT144) have been reported to have skeletal abnormalities,[11–21] mainly including a short thorax and limbs[11–15,17,18] and abnormalities in the shape of the epiphyseal plate,[13–18,20] the level of bone mineralization,[11,15,21] and the morphology and quantity of primary cilia.[12,14,15,17,19–21]

To reveal the underlying pathological mechanisms, several mutation or knockout mouse models of IFTs have been established.[15,21–23] Although ciliary misassembly and aberrant transmission of developmental signals, such as Hedgehog (HH) and Wnt signaling, are commonly accepted explanations for ciliopathies, several recent studies both in human case reports and in mouse models have suggested that each

Received for publication February 8, 2019; accepted May 23, 2019.

Corresponding Author:
Yao Sun, Department of Oral Implantology, School of Stomatology, Tongji University, Shanghai Engineering Research Center of Tooth Restoration and Regeneration, 399 Middle Yanchang Road, Shanghai 200072, China.
E-mail: yaosun@tongji.edu.cn

ciliary component may have distinct functions within or even outside the cilia.[24–27] Therefore, it is necessary to separately study the relationship between each IFT protein and bone development. Here, we focus on IFT140, a core protein of the IFT-A complex, in retrograde IFT, which has been identified in skeletal ciliopathies and Mainzer-Saldino and Jeune syndromes.[16,17] First, we found that the transcriptional level of Ift140 was downregulated in the long bones of aging- and ovariectomy (OVX)-induced osteoporotic mouse models. Furthermore, IFT140 showed characteristic expression in osteoblasts and chondrocytes at representative stages of bone development.

Materials and Methods

Mouse Models

All mice used were C57BL/6, and they were raised under standard animal housing conditions with free access to food and water. All experimentation using animals was approved by the animal experiment ethics committee of Tongji University (TJLAC-018-019). Two models of osteoporosis were used in this study: The mice in the aging group were naturally aging, 12-month-old C57BL/6 mice of either sex; 3-month-old C57BL/6 mice of either sex were used as the control group. For the OVX mice, the mice were ovariectomized (or sham-operated) at 2 months of age, and at 4 months after surgery, femurs from both groups were collected for total RNA extraction.

Cell Culture

For the primary cell cultures, osteoblasts, bone marrow mesenchymal stem cells (BMMSCs), and chondrocytes were cultured in α-MEM containing 10% FBS. For cell lines, MC-3T3-E1 (murine osteoblast-like cell line) was cultured in DMEM with 10% FBS, and MLO-Y4 (murine osteocyte-like cell line) was cultured in α-MEM containing 5% FBS and 5% calf serum (CS). All complete media contained penicillin (1 U/ml) and streptomycin (1 μg/ml), and all cell lines and primary cells were cultured at 37C in a humid incubator with 5% CO_2.

For the preparation of primary cells (osteoblasts, BMMSCs and chondrocytes), osteoblasts were isolated from mouse calvarial bone via a serial digestion method. In brief, 3-day postnatal C57BL/6 mice of either sex were sacrificed by decapitation and soaked in 75% ethanol for sterilization. Then, the calvarial bones were carefully dissected and subjected to sequential digestion with 2 mg/ml collagenase type I (Sigma-Aldrich; St Louis, MO) followed by 0.25% trypsin (Gibco; Grand Island, NY) at 37C for 10 min each. Next, the calvarial bones were cut into pieces and digested again in collagenase type I for 30 min. Cells and fragments were spun down and cultured in α-MEM complete medium. Primary BMMSCs and chondrocytes were isolated from bone marrow and articular cartilage of 4-week-old C57BL/6 mice long bones. After anesthesia by intraperitoneal infusion with 5% sodium pentobarbital, the mice were sacrificed, and femurs and tibias were dissected and cut open to expose the marrow cavity. The cell suspension was prepared by repeatedly rinsing the cavity with sterile PBS. The cells were collected by centrifugation and cultured in α-MEM complete medium. For chondrocyte isolation, the articular cartilage was removed from the femoral heads and digested in 0.25% trypsin at 37C for 10 min. Next, the cartilage was cut into pieces and digested in collagenase type II (2 mg/ml) for 1 hr, and the cells were spun down and washed with PBS before being plated in α-MEM complete medium.

In Vitro Osteogenic and Chondrogenic Induction of BMMSCs

To induce osteogenic or chondrogenic differentiation, third-generation BMMSCs were seeded in six-well plates with osteogenic or chondrogenic medium, respectively. The osteogenic medium was prepared by addition of dexamethasone (10 nM), β-glycerophosphate (5 mM), and ascorbic acid (50 μg/ml) to α-MEM complete medium. Chondrogenic induction was performed using a StemPro Chondrogenesis Differentiation Kit (Invitrogen; Grand Island, NY). The media were changed every 3 days. The cells were harvested for analysis of Ift140 and Runx2/Sox9 levels by real-time PCR every 3 days. Each experiment was conducted in triplicate.

Reverse Transcription Quantitative PCR (RT-qPCR) Analyses

RT-qPCR was performed to assess the mRNA expression levels of Ift140 in multiple organs, in femurs in various mouse models of osteoporosis, and in several types of bone cells. Total RNA from organ tissues and cultured cells was extracted using TRIzol Reagent (Invitrogen) per the manufacturer's instructions. First-strand cDNA was synthesized from 1 μg of total RNA in a final volume of 20 μl with oligo(dT) primers (Roche; Basel, Switzerland). The expression of target and internal reference genes was evaluated by RT-qPCR with a Fast Start Universal SYBR Green Master Kit (Roche, Switzerland). The primers used were as

follows: mouse Ift140: forward, 5′-CAGACCTGGACAG CACCATC-3′ and reverse, 5′-CAGTGCGCTGGTCC ACATAG-3′; mouse Runx2: forward, 5′-GCACAA ACATGGCCAGATTCA-3′ and reverse, 5′-AAGCCAT GGTGCCCGTTAG-3′; mouse Sox9: forward, 5′-AGC TCACCAGACCCTGAGAA-3′ and reverse, 5′-TCCC AGCAATCGTTACCTTC-3′; mouse GAPDH: forward, 5′-GGGAAGCCCATCACCATCTT-3′ and reverse, 5′-G CCTCACCCCATTTGATGTT-3′ (primers were synthesized by Invitrogen; Shanghai, China). The mouse GAPDH gene was used as an internal control for each sample. Four samples were collected from each group, and the reactions were run in triplicate. The relative mRNA expression levels of the genes were calculated using the $2^{-\Delta\Delta Ct}$ method.

Image Acquisition and Processing

For the imaging in tissue, a Nikon Eclipse 80i compound microscope with a Nikon DS-Ril camera (Nikon; Tokyo, Japan) was used, and NIS-Elements BR imaging software (version 4.20) was employed. To show the distribution of IFT140-positive cells in the long bone in a single view at high resolution, images (taking by 10× objective lens) were stitched together using the automatic photomerge tool of Adobe Photoshop.

Immunofluorescence Analysis

Mice of different ages were anesthetized, and then heart perfusions were performed with 4% paraformaldehyde (PFA). Long bone were removed, fixed (4% PFA, overnight), decalcified (10% EDTA for a month), and dehydrated (30% sucrose, overnight) before being embedded in OCT compound, and then 5 μm frozen sections were cut and subjected to immunofluorescence staining. Sections of different ages were stained in the same batch. Sections were blocked with 1% goat serum for 2 hr at room temperature, followed by incubation with primary antibody at 4C overnight. The sections were washed three times in PBS and then incubated with secondary antibodies (1:2000; Alexa Fluor 488 Goat Anti-Mouse IgG/Alexa Fluor 568 Goat Anti-Rabbit IgG; Invitrogen) for 1 hr at room temperature, away from light. Next, the sections were washed three times in PBS, mounted with ProLong Gold antifade reagent containing DAPI (Invitrogen), and coverslipped.

For dual immunofluorescence staining in vivo, the cilia axoneme was labeled by acetylated α-tubulin staining, and the cilia basal bodies were labeled by γ-tubulin staining. The acetylated α-tubulin antibody (produced in mouse, T6793; Sigma-Aldrich) and anti-γ-tubulin antibody (produced in rabbit, T3320; Sigma-Aldrich) were mixed and diluted (1:1000) as the primary antibodies. Similarly, to visualize the colocalization of IFT140 and cell cilia, antiacetylated α-tubulin (1:1000) antibody and anti-IFT140 antibody (1:500) were mixed and diluted as primary antibodies. All antibodies used were diluted in blocking buffer, and nonimmune IgG instead of the primary antibody was used as the negative control.

Morphometric Analysis and Quantification

Using ImageJ software, the mean percentages of IFT140-positive regions, both in growth plate chondrocytes and in trabecular osteoblasts, were calculated in 10 random fields (~20 cells in each field) for each immunofluorescence image. The positive signal threshold was set according to the signal intensity of the respective negative control image. The ratio of IFT140-positive signal in cells was calculated by dividing the measured IFT140-positive area by the total area of the cells (prohypertrophic chondrocytes and osteoblasts). To facilitate the illustration of IFT140 expression change at different growth stages and locations in the long bone, thresholds of 10%, 30%, 50%, and 70% were used to classify IFT140 expression levels into several grades: a ratio greater than 70% (++++), between 70% and 50% (+++), between 50% and 30% (++), between 10% and 30% (+), and less than 10% (+/–).

Statistical Analyses

Statistical analysis was performed using SPSS software 20.0. All values are expressed as mean ± SEM. The statistical significance between the two groups was assessed using Student's *t*-test. A value of $p<0.05$ was considered significant.

Results

Expression of IFT140 in Osteogenesis-related Cells

We first detected the mRNA expression levels of Ift140 in heart, liver, lung, kidney, eye, paranephros, bone, and tooth. In addition, in comparison with various soft tissue organs, Ift140 was abundantly expressed in bone and tooth, which are hard tissues (Fig. 1A). In bone, the expression of Ift140 was particularly prominent at 5- to 10-fold higher than in major soft tissues (Fig. 1A). To clarify whether IFT140 is related to bone disease, we further verified its expression in two

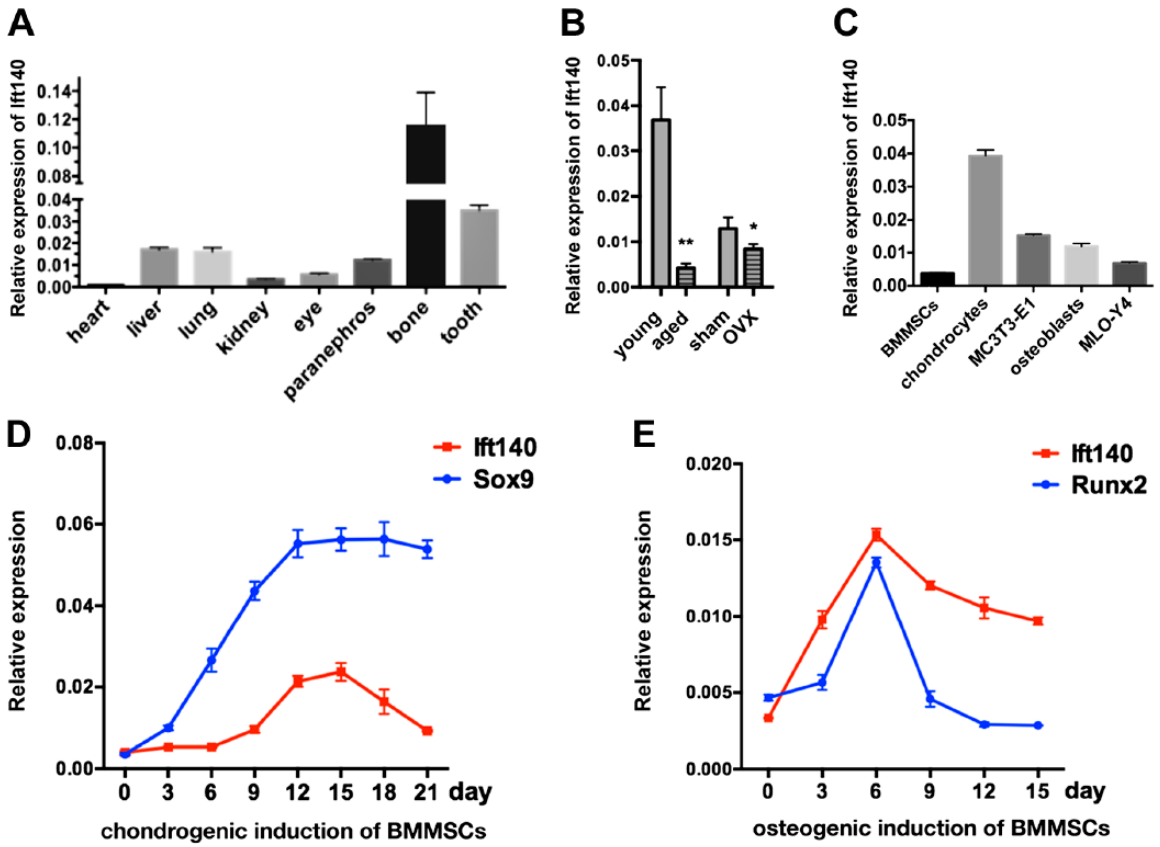

Figure 1. Expression characteristics of IFT140 in osteogenesis-related cells. (A) The mRNA expression level of Ift140 in the organs of 1-week-old mice, *n*=4. (B) RT-qPCR shows the mRNA expression of IFT140 in mouse femurs of two osteoporosis models compared with controls. Young and aged, 3-month-old and 12-month-old, C57BL/6 mice; sham and OVX, 6-month-old female C57BL/6 mice, 4 months after sham surgery or oophorectomy; *n*=4 in each group. (C) The mRNA expression of Ift140 in cultured bone cells, BMMSCs, primary chondrocytes, MC-3T3-E1 (murine osteoblast-like cell line), primary osteoblasts, and MLO-Y4 (murine osteocyte-like cell line). (D and E) The mRNA expression levels of Ift140 and early differentiation markers (Sox9, Runx2) during chondrogenetic/osteogenic induction of BMMSCs. The abscissa indicates the induction time in days. The values of target genes were normalized to GAPDH. Cell samples were collected every 3 days; error bars represent SEM. Abbreviations: RT-qPCR, reverse transcription quantitative PCR; OVX, ovariectomy; BMMSCs, bone marrow mesenchymal stem cells; SEM, standard error of the mean. **p*<0.05, ***p*<0.01, and ****p*<0.001, as determined by Student's *t*-test.

classical osteoporosis models (naturally aging and OVX mouse models) and found that Ift140 was significantly downregulated in bone disease groups compared with control groups (Fig. 1B).

To characterize the expression levels of Ift140 among bone cells responsible for bone formation, the expression of Ift140 in several types of primary cells (BMMSCs, preosteoblasts, chondrocytes) or cell lines (MC-3T3-E1 and MLO-Y4) was assessed. The results showed the highest expression in chondrocytes and the lowest expression in undifferentiated mesenchymal stem cells, with intermediate expression in osteoblasts (Fig. 1C). During chondrogenic and osteogenic inductions of mesenchymal stem cells, the expression patterns of Ift140 were consistent with the trends of Sox9 and Runx2, which are early markers for chondrogenic and osteogenic differentiation (Fig. 1D and E).

Subcellular Localization of IFT140 in Chondrocytes and Subchondral Osteoblasts In Vivo

As chondrocytes and preosteoblasts are the two cell types with the highest expression of IFT140, and early osteogenesis and chondrogenesis were the periods with high expression of Ift140, we next examined the subcellular expression of IFT140 in chondrocytes and subchondral osteoblasts in vivo. By double-labeling

immunofluorescence staining, the presence of cilia can be detected in both chondrocytes (embryonic mice long bone) and subchondral osteoblasts (2-week-old mice long bone) in tissue, as acetylated α-tubulin specifically labels the axoneme (green) and γ-tubulin specifically labels the basal body (red) of cilia (Fig. 2A and B). Moreover, colocalization of IFT140 and acetylated α-tubulin could be observed both in chondrocytes (Fig. 2C, E, and G) and in subchondral osteoblasts (Fig. 2D, F, and H). In addition, a large amount of IFT140-positive signals could be detected in the cytoplasm (Fig. 2G and H), which suggested that the distribution of IFT140 in these two types of cells might not be limited to cilia.

Expression of IFT140 in Long Bone During Embryonic Development

Next, at the histological level, we detected the expression and localization of IFT140 in mouse long bones at several representative stages of bone development. At embryonic day 12.5, IFT140 was weakly expressed in condensed mesenchymal cells of limb buds that give rise to the future cartilage primordium (Fig. 3B). At embryonic day 16.5, embryonic chondro-osseous rudiment was already formed, and high expression of IFT140 could be observed in hypertrophic chondrocytes and preosteoblasts around the perichondrium (Fig. 3E).

Expression of IFT140 in Postnatal Long Bone

After birth, the temporal and spatial expression of IFT140 in long bone was evaluated at different developmental stages, including newborn (the first ossification center is basically formed, Fig. 4A), week 1 (the secondary ossification center begins to form, Fig. 4D), week 2 (the secondary ossification center is basically formed, Fig. 4G), week 4 (the rapid development period of long bone, Fig. 5A–E), and week 8 (mice enter the stage of sexual maturation, when bone begins to grow more slowly, Fig. 5F–J).

On the first day after birth, strong signals of IFT140 were detected in chondrocytes of the growth plate, and weak signals could also be observed in the subchondral bone of the trabecular area (Fig. 4A–C). At week 1, with the development of the growth plate, the chondrocytes were arranged in columns, and IFT140 was detected in almost all layers of chondrocytes in the growth plate (Fig. 4D and E). Compared with the newborn mice, the expression level of IFT140 was increased in the trabecular bone area (Fig. 4D and F). During this period, positive signals of IFT140 appeared in differentiated chondrocytes of the epiphyseal plate near the future secondary ossification center area (indicated by asterisk in Fig. 4D). At week 2, the IFT140 stained area in the future secondary ossification center area gradually expanded. In addition, the distribution of IFT140-positive cells in the growth plate was uneven. In general, the staining persisted in areas of both the proliferative zone and prehypertrophic zone of the growth plate (Fig. 4H), which was much stronger than the hypertrophic zone near the calcified layer (Fig. 4J), and IFT140 expression was much stronger in subchondral bone cells than in chondrocytes (Fig. 4J and K).

At week 4, the expression levels of IFT140 in both the chondrocytes of the growth plate and bone cells of subchondral trabeculae decreased compared with week 2. In addition, the expression in newly formed bone tissue in the secondary ossification center increased (Fig. 5A–E). At week 8 (Fig. 5F–J), bone development entered a slower phase, when only a small fraction of chondrocytes retained IFT140-positive staining. In contrast, despite a visible decrease in its expression, IFT140 signals could also be clearly observed on the surface of trabecular bone under the growth plate and in the secondary ossification center.

Evaluation of IFT140 Expression Levels During Bone Development

To further summarize the dynamic change in IFT140 expression in both trabecular and cartilage tissue with time, we conducted fluorescence quantification, and the data are summarized in Table 1. For the trabecular region, the IFT140 signal in osteoblasts was weak at birth (+/–, 7.66%), reached a peak at the week 1 (++++, 84.93%), decreased at week 2 (+++, 68.86%), and then stabilized after 4 weeks of age (++, 41.73%). For the cartilage region, after birth, the IFT140 signal was strongest (++, 42.25%) in prehypertrophic chondrocytes in the growth plate, then decreased gradually (++, 38.33%), and was maintained at a low level after 4 weeks of age (+/–, around 3%). In the epiphysis, a weak signal could be observed in chondrocytes at week 1 (+, 22.86%), which was enhanced 1 week later (+, 32.25%). At week 4, when most of the highly differentiated cartilage cells were replaced by bone remodeling, low expression of IFT140 (+/–, 8.23%) was observed in the remaining chondrocytes. In brief, the expression level of IFT140 occurred in waves, with expression peaks observed in turn in chondrocytes and osteoblasts, which is consistent with the representative stages during bone development.

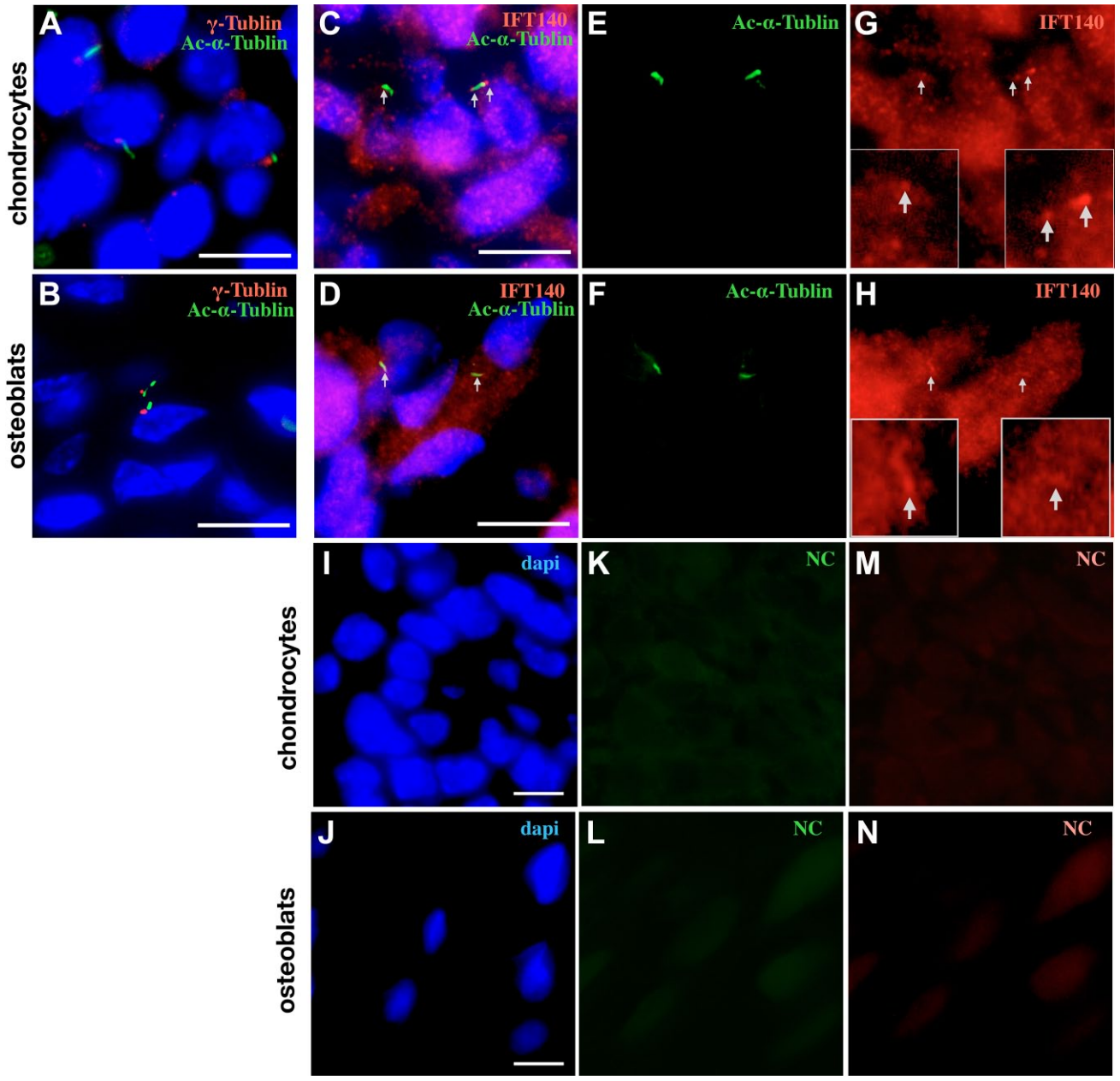

Figure 2. Subcellular location of IFT140 shown by immunofluorescence staining. (A and B) The cilia of chondrocytes (A) and subchondral osteoblasts (B) were costained with acetylated α-tubulin (green) and γ-tubulin (red). (C–H) The subcellular localization of IFT140 in chondrocytes (C, E, G) and subchondral osteoblasts (D, F, H); images of the red, green, and blue channels are presented, respectively; the green channel images (E and F) show acetylated α-tubulin; the red channel images (G and H) show IFT140 signal, and the magnified regions of the cilia are shown in boxes; nuclei were visualized by DAPI staining (blue); C and D are merged images; colocalization of IFT140 and acetylated α-tubulin was indicated by arrows. (I–M) Three-channel luminescent images of the NC group, the chondrocytes (I, K, L), and subchondral osteoblasts (J, L, M). Scale bar = 10 μm. Abbreviation: NC, negative control.

To better understand the correlation between cilia and cytoplasmic localization of IFT140, double immunofluorescence costaining of cilia (acetylated α-tubulin) and IFT140 at four representative time-points (week 1, week 2, week 4, and week 8) of postnatal long bone growth was performed (Fig. 6). In the growth plates, the ciliated cells have been observed between the proliferative layer and the prehypertrophic layer, and cells with strong cytoplasmic staining of IFT140 have been found mostly in the prehypertrophic and hypertrophic layers (Fig. 6A). In subchondral bone, ciliary structures can be observed in only a few of the bone cells (Fig. 6B).

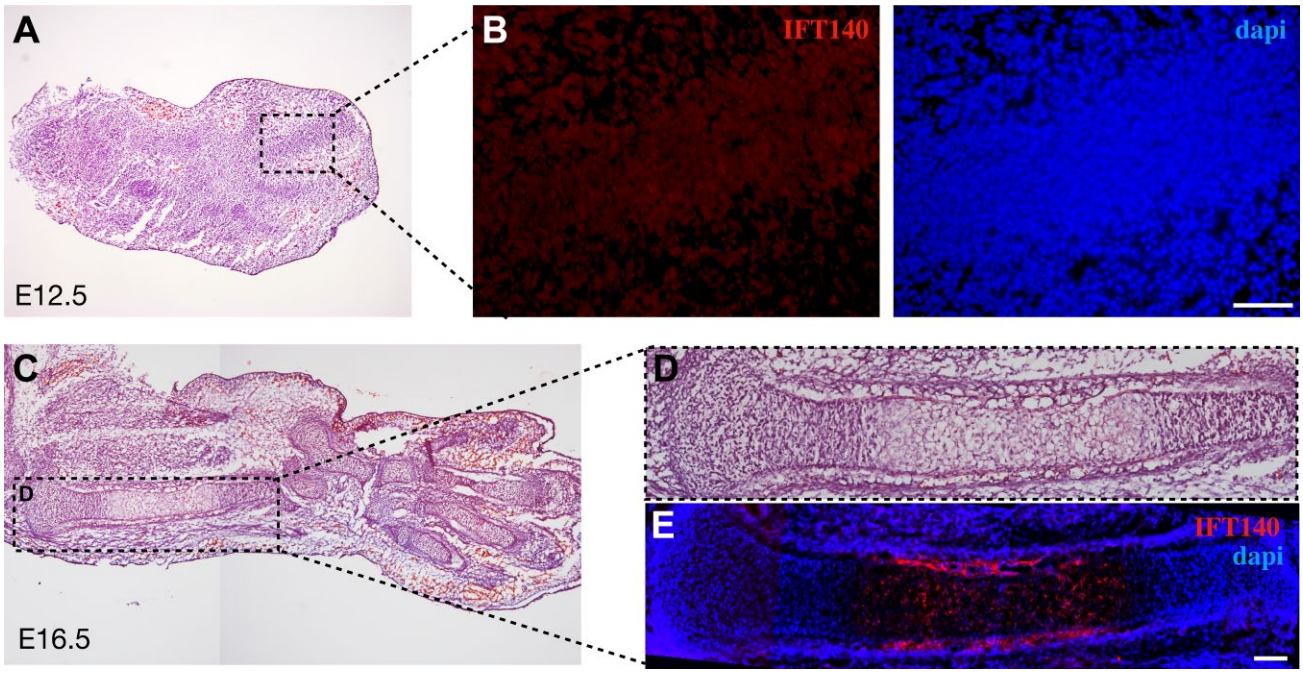

Figure 3. Expression of IFT140 in mouse long bone during embryonic development. (A) H&E staining of mouse limb bud at embryonic day 12.5. (B) immunofluorescence staining showing the expression of IFT140 (red) with DAPI staining (blue) in the boxed region of (A). (C) H&E staining of mouse upper limb at embryonic day 16.5. (D) Magnified image of the boxed region in (C). (E) Immunofluorescence staining of IFT140 (red) and DAPI staining (blue), the same position as shown in (D). Figs. 3C–E are stitched images. Scale bar = 100 μm.

Discussion

Bone morphogenesis is the result of bone progenitor cells working in orders orchestrated by various developmental signaling. Some key signaling pathways, such as HH and Wnt, are mediated by the correct assembly of cilia, which depends on IFT.[28,29] Thus far, alterations of several IFT genes, both in humans and in animal models, have suggested that IFT plays an essential role in bone development.[11,15–18,22,23] It is known that some components of the IFT-B complex can regulate osteogenesis. Deletions of these genes (*IFT80* and *IFT88*) in osteoblast precursor cells disrupt primary cilia and block osteoblast differentiation.[22,23] However, little is known about how IFT-A complex members are involved in bone developmental processes.

In this study, we investigated the expression pattern of IFT140, a core protein of the IFT-A complex, during bone development. The results showed that, compared with most of the soft tissue organs, IFT140 was highly expressed in bone (Fig. 1A). Moreover, its expression was downregulated in the long bones of mice with aging- and OVX-induced bone loss (Fig. 1B). Furthermore, the expression of IFT140 was correlated with bone formation markers during the differentiation of BMMSCs (Fig. 1D and E). These data suggest that IFT140 may play a specific role during bone formation.

On further investigation, in the middle stage of embryo development (chondrogenesis and perichondrium formation stage), IFT140 was strongly expressed in the differentiated chondrocytes and preosteoblasts around the perichondrium (Fig. 3E). After birth, when the primary ossification center had formed, IFT140 expression had increased significantly. At week 2, the expression of IFT140 in chondrocytes of the growth plate became weaker than at the earlier timepoints, was maintained at a high level in the trabecular bone area of rapid osteogenesis, and then decreased after the period of rapid growth and development (Figs. 3–5 and Table 1). In summary, IFT140 expression was found to be involved in crucial stages of endochondral ossification and was present in active chondrocytes and osteoblasts near chondrogenic–osteogenic interfaces. These findings suggest that IFT140 might be closely related to the process of endochondral bone formation and it may serve as a development indicator of rapid growth, both in cartilage and in trabeculae of long bone.

Given that some IFTs have been found to regulate activities of bone cells, they are involved in cartilage

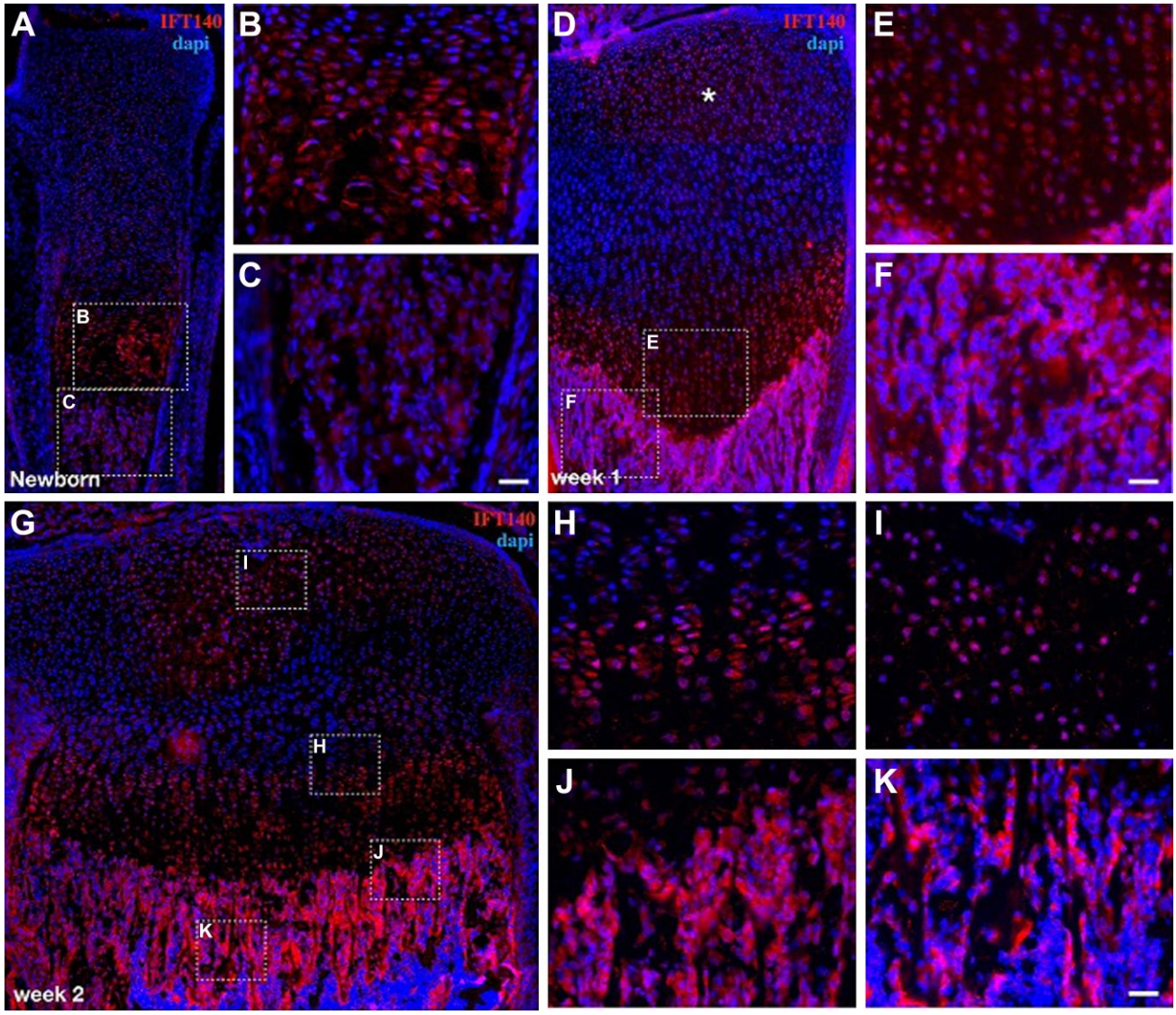

Figure 4. Expression of IFT140 in newborn, 1, and 2-week-old mouse long bone. (A, D, G) The expression of IFT140 in newborn, 1, and 2-week-old mouse tibia (immunofluorescence staining). (B, C, E, F, H–K) The boxed regions in (A), (D), and (G) were magnified and are shown on the right. Asterisk in (D) marks the site where the future second ossification center will form. Figs. 4A, 4D, and 4G are stitched images. Scale bar = 50 μm.

and bone formation[22,23,30]; in patients, IFT140 mutations lead to short stature and insufficient rib growth leading to a narrow thorax;[16–18] for cauli,[21] a mouse model with a recessive missense mutation in the *Ift140* gene also exhibits severe skeletal malformation, all of which are associated with the process of endochondral ossification. Therefore, the characteristic expression of IFT140 during endochondral osteogenesis will provide ideas for revealing the pathogenic mechanisms of skeletal ciliopathies.

Herein, at the subcellular level, IFT140 was found localized in both cilia (tip and base) and cytoplasm of chondrocytes and subchondral osteoblasts (Fig. 2A and B). In the growth plate, chondrocytes arrange through sequential differentiation steps in columns, and cilia have been observed mainly in cells between the proliferative layer and the prehypertrophic layer (Fig. 6A), which indicates the requirement for cilia at a specific phase during chondrocyte hypertrophy. Moreover, IFT140 expression was more extensive than cilia distribution (Fig. 6A); while the strong positive cells of IFT140 were mainly concentrated in the hypertrophic layer (Fig. 6A), the ciliary cells and IFT140 strong positive cells partially, but not

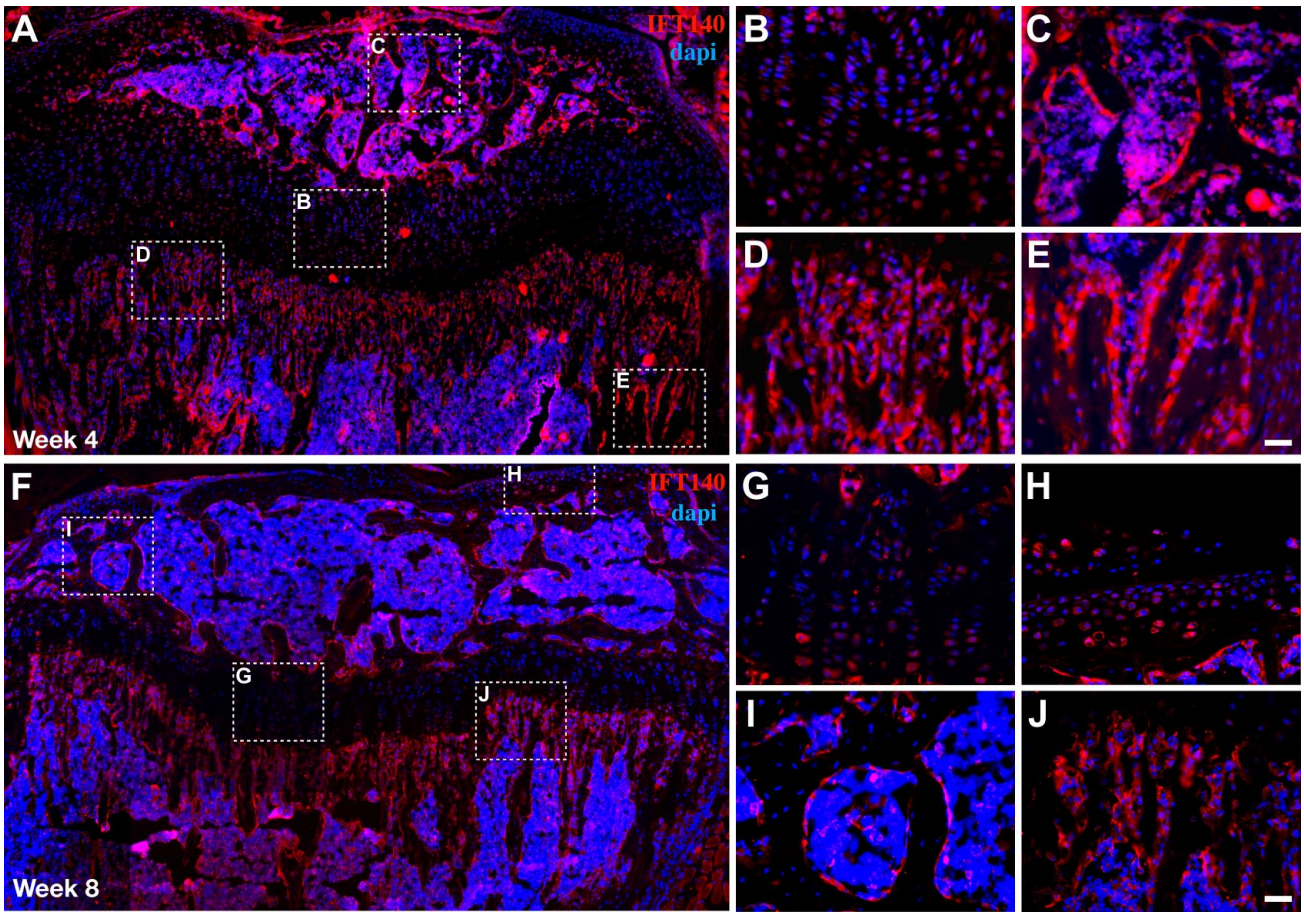

Figure 5. Expression of IFT140 in 4- and 8-week-old mouse long bone. (A and F) Images of immunofluorescence staining showing the IFT140 signal in 4- and 8-week-old mouse tibia. (B–E and H–K) The boxed regions in (A) and (F) were magnified and are shown on the right. Figs. 5A and 5F are stitched images. Scale bar = 50 μm.

Table 1. Quantitative Assessment of IFT140-positive Signals in Chondrocytes and Trabecular Cells.

	Chondrocytes		Trabecular Cells	
	POC	SOC	POC	SOC
E16.5	+ (29.26)	N	N	N
Newborn	++ (42.25)	– (0.02)	+/– (7.66)	N
Week 1	++ (38.33)	+ (22.86)	++++ (84.93)	N
Week 2	+ (13.33)	+ (32.25)	+++ (68.86)	N
Week 4	+/– (3.77)	+/– (8.23)	++ (41.73)	+++ (59.75)
Week 8	+/– (2.96)	+/– (6.73)	++ (35.57)	++ (44.50)

"++++"and "+++," strong positive; "++," moderate positive; "+"and "+/–," low; "–," negative; "N," no such type of cell here. The numbers in parentheses represent the mean percentage of IFT140-positive signals in the cell.
Abbreviations: POC, primary ossification center; SOC, secondary ossification center; E16.5, embryonic day 16.5.

completely, overlapped in the columnar regions of the growth plate. Similarly, in the subchondral bone cells, only a few IFT140-positive cells exhibited cilia (Fig. 6B). The mismatch of IFT140 expression and cilia distribution may be, on one hand, due to the fact that not all cilia can be observed at the histological level in tissue. On the other hand, it may not exclude the possibility of an independent role of IFT140 in cytoplasm as postulated in "the functions outside cilia theory" of IFTs. Cilia are extensions of the cytoskeleton, and an increasing number of ciliary proteins have been found to serve functions outside cilia. For example, IFT20 has been found to be responsible for transport between the Golgi complex and the base of the cilium, during which the involvement of IFT140 is necessary[27]; some IFTs are also associated with exocytosis even in cells without cilia.[31] These indications led us to speculate that IFT140, to some extent, might serve distinct roles that are not exclusive to cilia (e.g., mediating matrix vesicle transport), and the potential functions remain to be revealed.

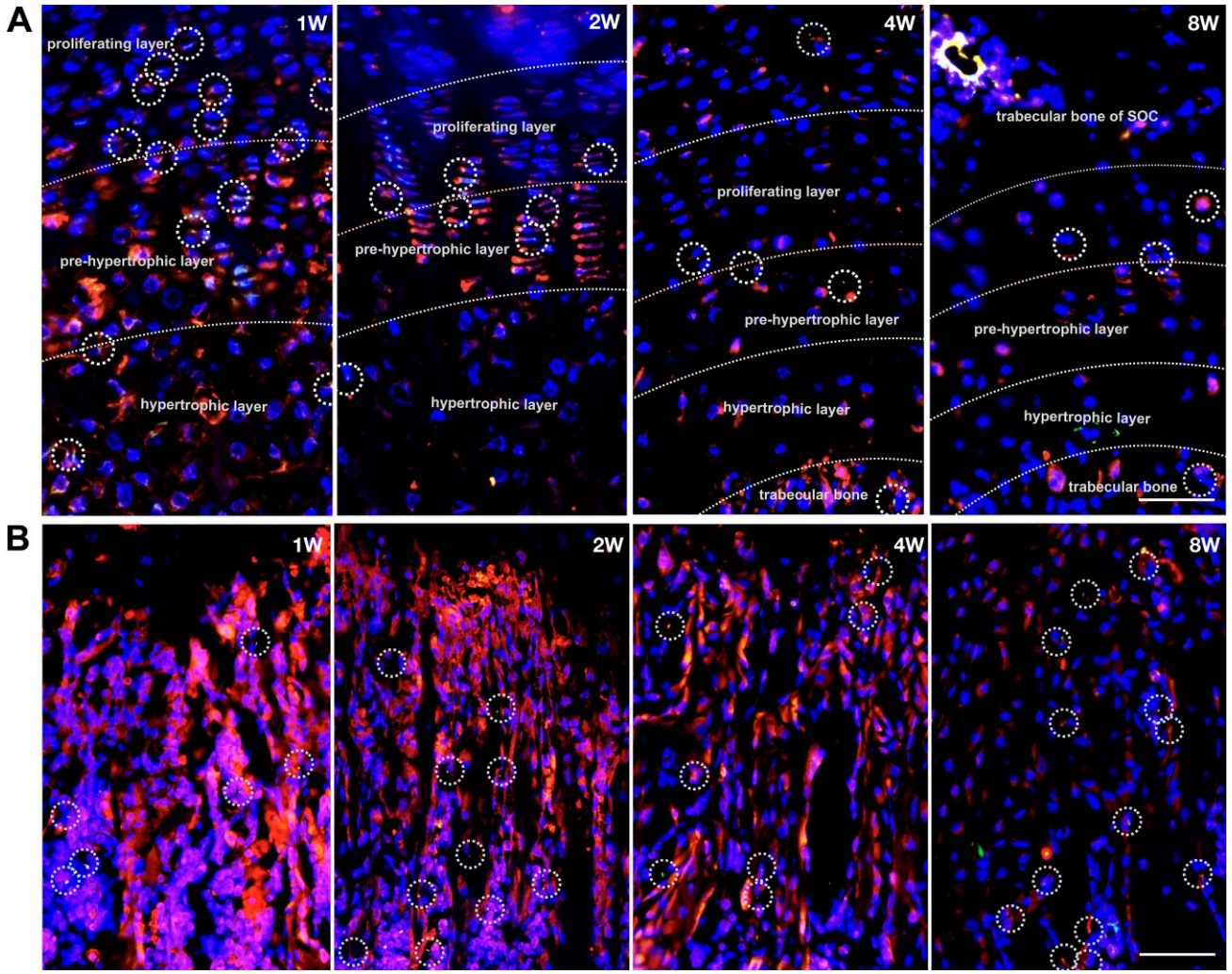

Figure 6. Distribution of IFT140-positive cells and ciliary cells in postnatal mice long bones. (A and B) Immunofluorescence images of mice growth plates (A) and subchondral trabecular bone (B) at four representative timepoints (week 1, week 2, week 4 and week 8): IFT140 (red) and acetylated α-tubulin (green); the chondrocytes in series of differentiation and activity phases were divided by dotted lines; typical cilia were delineated with circles. Scale bar = 100 μm. Abbreviation: SOC, secondary ossification center.

Competing Interests

The author(s) declared no potential conflicts of interest with respect to the research, authorship, and/or publication of this article.

Author Contributions

All authors have contributed to this article as follows: CZ and YS designed the experiments and organized the manuscript. CZ and SZ performed the experiments, and CZ and YS analyzed the data. All authors reviewed the manuscript.

Funding

The author(s) disclosed receipt of the following financial support for the research, authorship, and/or publication of this article: This study was founded by Key Project of Chinese National Programs for Research of Development (2016YFC1102705, Y.S.), National Science Foundation of China (81822012, 81470715, and 81771043, Y.S.), Shanghai Health System (2017 BR009, Y.S.), and Basic Scientific Research Operating Expenses of Central Universities—Interdisciplinary Research Project of Tongji University (20173386).

Literature Cited

1. Wheatley DN, Wang AM, Strugnell GE. Expression of primary cilia in mammalian cells. Cell Biol Inter. 2013;20(1):73–81.
2. Christensen ST, Pedersen LB, Schneider L, Satir P. Sensory cilia and integration of signal transduction

in human health and disease. Traffic. 2010;8(2):97–109.
3. Veena S, Reiter JF. The primary cilium as the cell's antenna: signaling at a sensory organelle. Science. 2006;313(5787):629–633.
4. Berbari NF, O'Connor AK, Haycraft CJ, Yoder BK. The primary cilium as a complex signaling center. Curr Biol. 2009;19(13):R526–R535.
5. Hiroaki I, Marshall WF. Ciliogenesis: building the cell's antenna. Nature Rev Mole Cell Biol. 2011;12(4):222–234.
6. Hoey DA, Chen JC, Jacobs CR. The primary cilium as a novel extracellular sensor in bone. Front Endocrinol. 2012;3:75.
7. Pedersen LB, Rosenbaum JL. Chapter two intraflagellar transport (IFT): role in ciliary assembly, resorption and signalling. Curr Topic Develop Biol. 2008;85(85):23–61.
8. Waters AM. Ciliopathies: an expanding disease spectrum. Pediat Nephrol. 2011;26(7):1039–1056.
9. Celine H, Valerie CD. Ciliary disorder of the skeleton. Am J Med Genet Part C Sem Med Genet. 2012;160C(3):165–174.
10. Mitchison HM, Valente EM. Motile and non-motile cilia in human pathology: from function to phenotypes. J Pathol. 2017;241(2):294.
11. Mill P, Lockhart PJ, Fitzpatrick E, Mountford HS, Hall EA, Reijns MA, Keighren M, Bahlo M, Bromhead CJ, Budd P, Aftimos S, Delatycki MB, Savarirayan R, Jackson IJ, Amor DJ. Human and mouse mutations in WDR35 cause short-rib polydactyly syndromes due to abnormal ciliogenesis. Am J Human Genet. 2011;88(4):508–515.
12. Walczak-Sztulpa J, Eggenschwiler J, Osborn D, Brown DA, Emma F, Klingenberg C, Hennekam RC, Torre G, Garshasbi M, Tzschach A, Szczepanska M, Krawczynski M, Zachwieja J, Zwolinska D, Beales PL, Ropers HH, Latos-Bielenska A, Kuss AW. Cranioectodermal Dysplasia, Sensenbrenner syndrome, is a ciliopathy caused by mutations in the IFT122 gene. Am J Human Genet. 2010;86(6):949–956.
13. Gilissen C, Arts HH, Hoischen A, Spruijt L, Mans DA, Arts P, van Lier B, Steehouwer M, van Reeuwijk J, Kant SG, Roepman R, Knoers NV, Veltman JA, Brunner HG. Exome sequencing identifies WDR35 variants involved in Sensenbrenner syndrome. Am J Human Genet. 2010;87(3):418–423.
14. Arts HH, Bongers EM, Mans DA, van Beersum SE, Oud MM, Bolat E, Spruijt L, Cornelissen EA, Schuurs-Hoeijmakers JH, de Leeuw N, Cormier-Daire V, Brunner HG, Knoers NV, Roepman R. C14ORF179 encoding IFT43 is mutated in Sensenbrenner syndrome. J Med Genet. 2011;48(6):390.
15. Ashe A, Butterfield NC, Town L, Courtney AD, Cooper AN, Ferguson C, Barry R, Olsson F, Liem KF Jr, Parton RG, Wainwright BJ, Anderson KV, Whitelaw E, Wicking C. Mutations in mouse Ift144 model the craniofacial, limb and rib defects in skeletal ciliopathies. Human Mole Genet. 2012;21(8):1808–1823.
16. Perrault I, Saunier S, Hanein S, Filhol E, Bizet AA, Collins F, Salih MA, Gerber S, Delphin N, Bigot K, Orssaud C, Silva E, Baudouin V, Oud MM, Shannon N, Le Merrer M, Roche O, Pietrement C, Goumid J, Baumann C, Bole-Feysot C, Nitschke P, Zahrate M, Beales P, Arts HH, Munnich A, Kaplan J, Antignac C, Cormier-Daire V, Rozet JM. Mainzer-Saldino syndrome is a ciliopathy caused by IFT140 mutations. Am J Human Genet. 2012;90(5):864–870.
17. Schmidts M, Frank V, Eisenberger T, Al Turki S, Bizet AA, Antony D, Rix S, Decker C, Bachmann N, Bald M, Vinke T, Toenshoff B, Di Donato N, Neuhann T, Hartley JL, Maher ER, Bogdanović R, Peco-Antić A, Mache C, Hurles ME, Joksić I, Guć-Šćekić M, Dobricic J, Brankovic-Magic M, Bolz HJ, Pazour GJ, Beales PL, Scambler PJ, Saunier S, Mitchison HM, Bergmann C. Combined NGS approaches identify mutations in the intraflagellar transport gene IFT140 in skeletal ciliopathies with early progressive kidney disease. Human Mut. 2013;34(5):714–724.
18. Khan AO, Bolz HJ, Bergmann C. Early-onset severe retinal dystrophy as the initial presentation of IFT140-related skeletal ciliopathy. J Am Assoc Pediat Ophthalmol Strabismus. 2014;18(2):203–205.
19. Davis EE, Zhang Q, Liu Q, Diplas BH, Davey LM, Hartley J. TTC21B contributes both causal and modifying alleles across the ciliopathy spectrum. Nature Genet. 2011;43(3):189–196.
20. Bredrup C1, Saunier S, Oud MM, Fiskerstrand T, Hoischen A, Brackman D, Leh SM, Midtbø M, Filhol E, Bole-Feysot C, Nitschké P, Gilissen C, Haugen OH, Sanders JS, Stolte-Dijkstra I, Mans DA, Steenbergen EJ, Hamel BC, Matignon M, Pfundt R, Jeanpierre C, Boman H, Rødahl E, Veltman JA, Knappskog PM, Knoers NV, Roepman R, Arts HH. Ciliopathies with skeletal anomalies and renal insufficiency due to mutations in the IFT-A gene WDR19. Am J Hum Genet. 2011;89(5):634–643.
21. Miller KA1, Ah-Cann CJ, Welfare MF, Tan TY, Pope K, Caruana G, Freckmann ML, Savarirayan R, Bertram JF, Dobbie MS, Bateman JF, Farlie PG. Cauli: a mouse strain with an Ift140 mutation that results in a skeletal ciliopathy modelling Jeune syndrome. PLoS Genetics. 2013;9(8):e1003746.
22. Yuan X, Cao J, He X, Serra R, Qu J, Cao X, Yang S. Ciliary IFT80 balances canonical versus non-canonical hedgehog signalling for osteoblast differentiation. Nature Commun. 2016;7:11024.
23. Haycraft CJ, Zhang Q, Song B, Jackson WS, Detloff PJ, Serra R, Yoder BK. Intraflagellar transport is essential for endochondral bone formation. Development. 2007;134(2):307–316.
24. May-Simera HL. Cilia, Wnt signaling, and the cytoskeleton. Cilia. 2012;1(1):7.
25. Mukhopadhyay S, Wen X, Chih B, Nelson CD, Lane WS, Scales SJ, Jackson PK. TULP3 bridges the IFT-A complex and membrane phosphoinositides to promote trafficking of G protein-coupled receptors into primary cilia. Genes Develop. 2010;24(19):2180–2193.
26. Finetti 1, Paccani SR, Riparbelli MG, Giacomello E, Perinetti G, Pazour GJ, Rosenbaum JL, Baldari CT.

Intraflagellar transport is required for polarized recycling of the TCR/CD3 complex to the immune synapse. Nature Cell Biol. 2009;11(11):1332–1339.
27. Crouse JA, Lopes VS, Sanagustin JT, Keady BT, Williams DS, Pazour GJ. Distinct functions for IFT140 and IFT20 in opsin transport. Cell Motil Cytoskeleton. 2014;71(5):302–310.
28. Zhu J, Nakamura E, Nguyen MT, Bao X, Akiyama H, Mackem S. Uncoupling sonic hedgehog control of pattern and expansion of the developing limb bud. Develop Cell. 2008;14(4):624–632.
29. Danwei H, Aimin L, Rakeman AS, Murcia NS, Lee N, Anderson KV. Hedgehog signalling in the mouse requires intraflagellar transport proteins. Nature. 2003;426(6962):83–87.
30. Yuan X, Serra RA, Yang S. Function and regulation of primary cilia and intraflagellar transport proteins in the skeleton. Ann New York Acad Sci. 2015;1335(1):78–99.
31. Baldari CT, Rosenbaum J. Intraflagellar transport: it's not just for cilia anymore. Curr Opin Cell Biol. 2010;22(1):75–80.